Electronic Supplementary Material (ESI) for Journal of Materials Chemistry C.

SUPPORTING INFORMATION

Charge transfer complexes of a benzothienobenzothiophene derivative and their implementation as active layer in solution-processed thin film organic field-effect transistors

Lamiaa Fijahi, Tommaso Salzillo*, Adrián Tamayo, Marco Bardini, Christian Ruzié, Claudio Quarti, David Beljonne*, Simone d'Agostino*, Yves Geerts, Marta Mas-Torrent*

Table S1. Crystal data and refinement details for crystalline (C_8O-BTBT-OC_8)(F_2TCNQ) and (C_8O-BTBT-OC_8)(F_4TCNQ).

	(C_8O-BTBT-OC_8)(F_2TCNQ)	**(C_8O-BTBT-OC_8)(F_4TCNQ)**
Formula	$C_{42}H_{42}F_2N_4O_2S_2$	$C_{42}H_{40}F_4N_4O_2S_2$
FW (g/mol)	736.91	772.90
Temperature/K	200	200
Crystal system	Triclinic	Triclinic
Space group	P-1	P-1
***a*/Å**	6.990(3)	6.920(2)
***b*/Å**	7.879(3)	8.024(1)
***c*/Å**	18.150(5)	18.043(3)
α/°	88.77(2)	89.08(1)
β/°	83.18(3)	82.89(2)
γ/°	72.80(3)	72.80(2)
Volume/Å^3	947.9(6)	949.7(3)
Z (Z')	1 (0.5)	1(0.5)
ρ_{calc} g/cm^3	1.291	1.351
μ/mm^{-1}	0.192	0.202
λ / Å	0.71073	0.07173
measd rflns	6028	7426
indep rflns	3344	4294
R_1	0.1036	0.0876
wR_2	0.3162	0.1817

Table S2 reports band dispersion and effective masses calculated on the reciprocal space directions which most closely match the real space crystallographic axes. In some cases precise values are not given because for very low band dispersion the calculation starts becoming unreliable. It is sufficient to know that the effective mass is several times larger than the standard electron mass, thus making charge transport in that direction highly unlikely.

Table S2: Bandwidth along all three crystallographic directions for the conduction band (CB) and valence band (VB) alongside the effective masses expressed with respect to the standard electron mass.

		Bandwidth (meV)		Effective mass (m*/m)	
Co-crystals	Cryst. Direction	CB	VB	Electrons	Holes
	X	357	174	1.8	3.1
(C_8O-BTBT-OC_8)(F_2TCNQ)	Y	44	33	>10	>10
	Z	0	0	Inf.	Inf.
	X	408	244	1.4	2.0
(C_8O-BTBT-OC_8)(F_4TCNQ)	Y	33	2	>10	>10
	Z	0	0	Inf.	Inf.

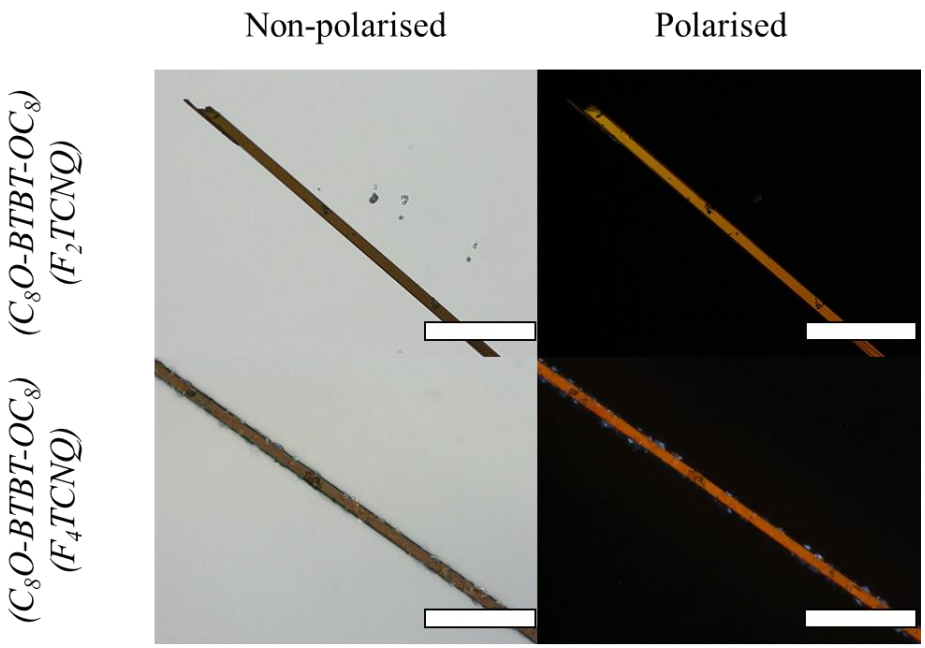

Figure S1. a) Polarised Optical microscopy images of (a) (C_8O-BTBT-OC_8)(F_2TCNQ) and (b) (C_8O-BTBT-OC_8)(F_4TCNQ). Scale bar: 100 μm

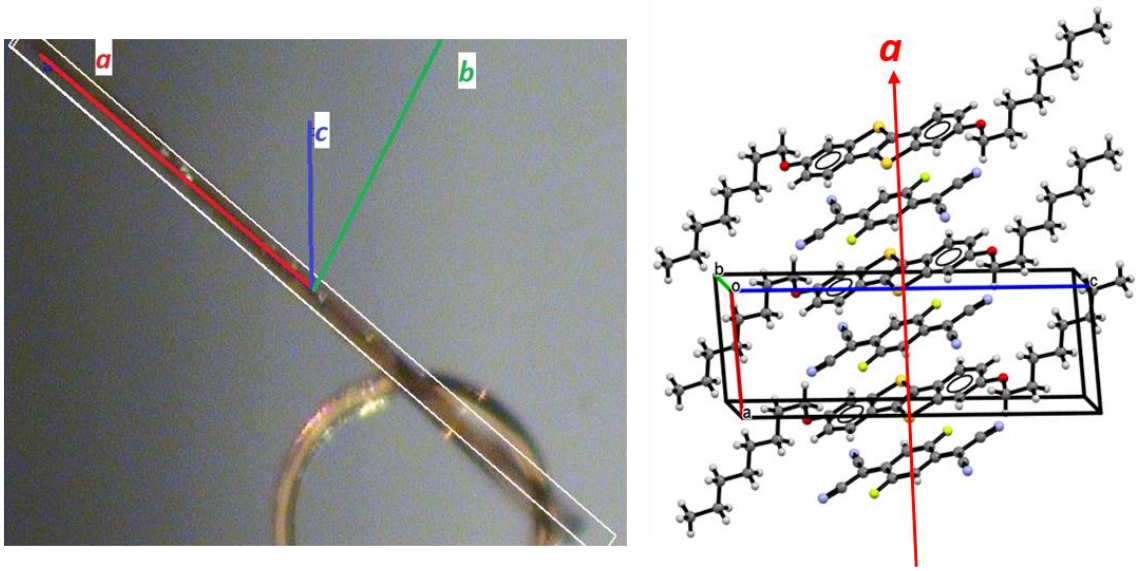

Figure S2. External morphology, experimentally determined, for a single crystal of (C_8O-BTBT-OC_8)(F_2TCNQ).

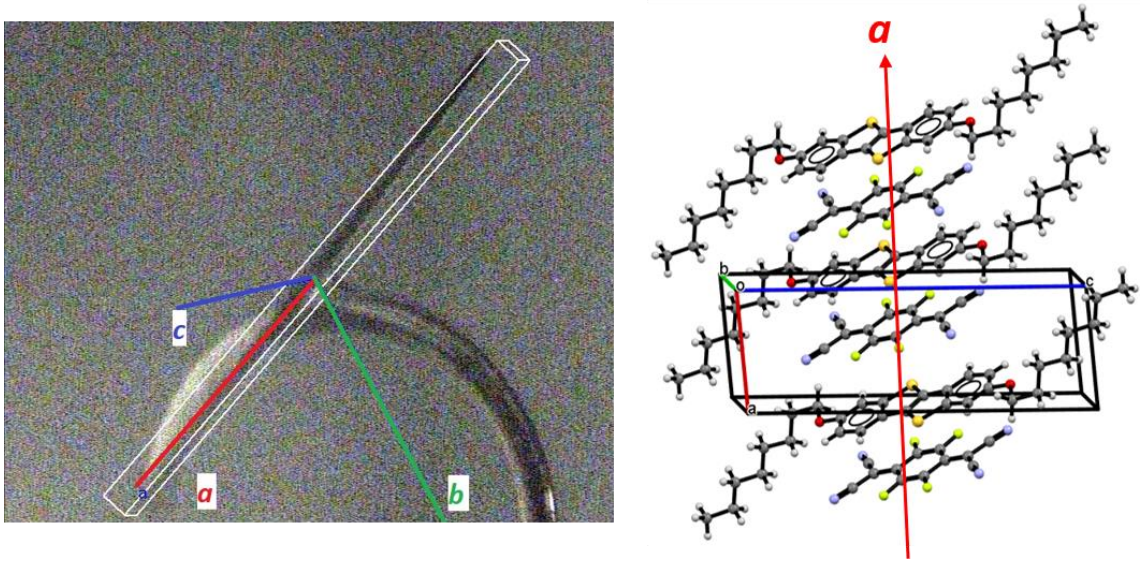

Figure S3. External morphology, experimentally determined, for a single crystal of (C_8O-BTBT-OC_8)(F_4TCNQ).

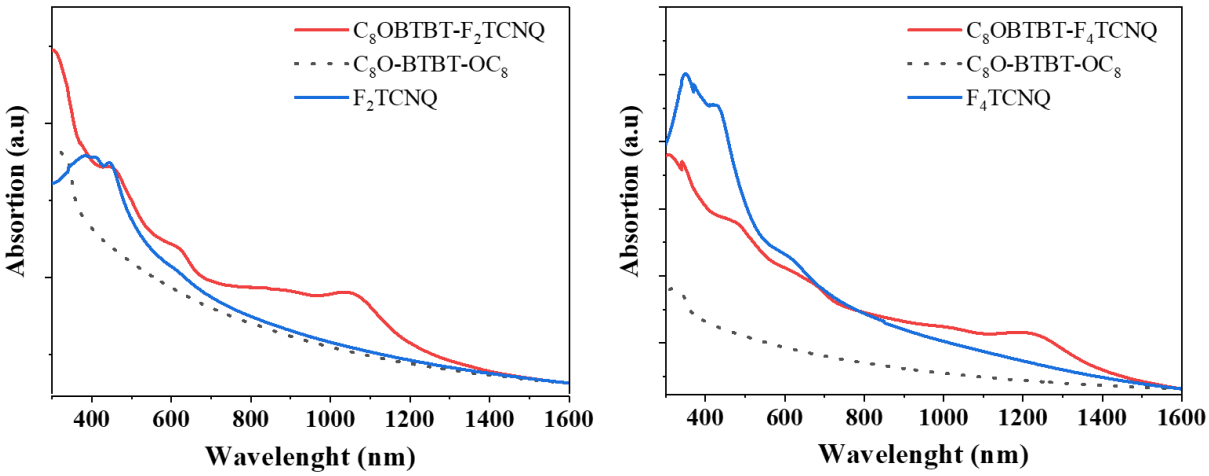

Figure S4. Left. UV-Vis-NIR absorption spectra in solid state of (C_8O-BTBT-OC_8)(F_2TCNQ), C_8O-BTBT-OC_8 and F_2TCNQ. Right. UV-Vis-NIR spectra in solid state of (C_8O-BTBT-OC_8)(F_4TCNQ), C_8O-BTBT-OC_8 and F_4TCNQ.

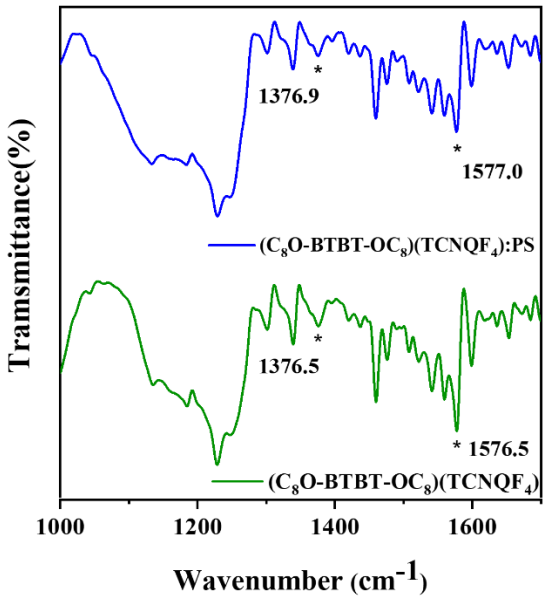

Figure S5. IRRAS spectra of (C_8O-BTBT-OC_8)(F_4TCNQ):PS and (C_8O-BTBT-OC_8)(F_4TCNQ) films. The possible C-C sensitive modes are marked with an asterisk.

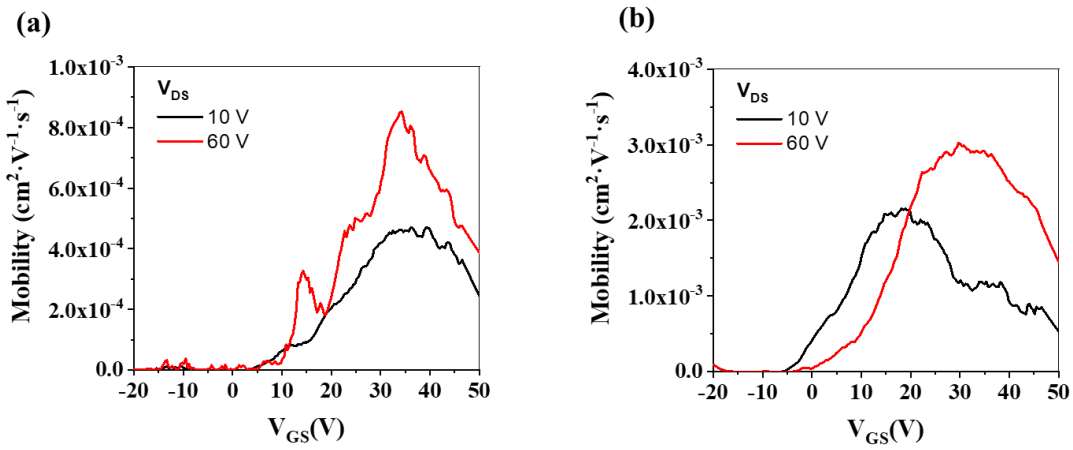

Figure S6. Mobility profiles in linear (VDS= 10 V) and saturation (VDS=60 V) regime as a function of the gate voltage for OFETs based on (a) (C8O-BTBT-OC8)(F4TCNQ) and (C8O-BTBT-OC8)(F4TCNQ):PS.

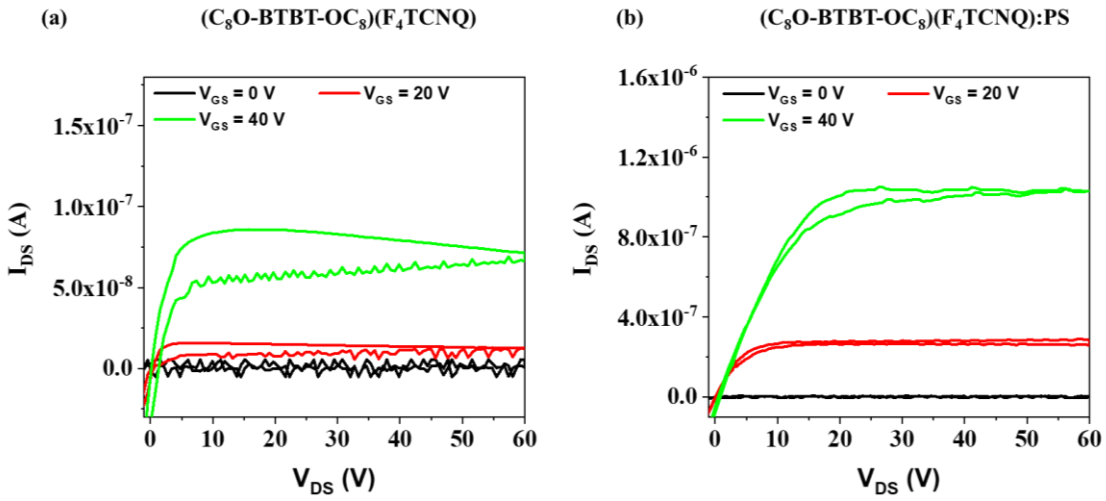

Figure S7. Output characteristics of the OFETs based on (a) (C_8O-BTBT-OC_8)(F_4TCNQ) and (C_8O-BTBT-OC_8)(F_4TCNQ):PS.